

Three-dimensional theory of superradiant free-electron lasers

River R. Robles,^{1,2,3,*} Luca Giannessi,^{4,5} and Agostino Marinelli^{1,3,†}

¹*SLAC National Accelerator Laboratory, Menlo Park, CA 94025*

²*Stanford University, Department of Applied Physics, Stanford, CA 94305*

³*Stanford PULSE Institute, SLAC National Accelerator Laboratory, Menlo Park, CA 94025, USA*

⁴*Elettra-Sincrotrone Trieste, 34149 Basovizza, Trieste, Italy*

⁵*ENEA C.R. Frascati, 00044 Frascati (Roma), Italy*

(Dated: March 19, 2024)

The soliton-like superradiant regime of free-electron lasers (FEL) offers a promising path towards ultrashort pulses, beyond the natural limit dictated by the bandwidth of the high-gain FEL instability. In this work we present a three-dimensional theory of the superradiant regime. Our work takes advantage of recent developments in non-linear FEL theory to provide a fully analytical description of soliton-like superradiance. Our theory proves the existence of a diffraction-dominated steady-state regime in which the superradiant peak power grows indefinitely while leaving the pulse duration and on-axis intensity almost unchanged. These results are in excellent agreement with three-dimensional simulations and are supported by recent experimental results at the Linac Coherent Light Source. This work advances non-linear FEL theory and provides a theoretical framework for the next generation of attosecond x-ray FELs.

X-ray free-electron lasers (XFELs) are unrivaled in their ability to produce short, high power x-ray pulses [1–5]. The recent development of attosecond XFELs [5–9] in particular has enabled the generation of isolated pulses with hundreds of attosecond duration and intensities surpassing table-top harmonic sources by six orders of magnitude. This enables novel applications combining attosecond time resolution with nonlinear spectroscopy [10] and single-particle imaging [11]. Achieving increasingly higher time-resolution and intensity requires a deeper exploration of non-linear FEL dynamics and the fundamental limits of short pulse generation.

In a high-gain FEL, a beam of relativistic electrons interacts with a co-propagating radiation pulse in a magnetic undulator [12, 13]. The resonant interaction between electrons and photons gives rise to a collective instability that amplifies exponentially the radiation power, and introduces a density modulation in the beam known as microbunching. In this context, the amplification bandwidth of the XFEL is determined by the relative slippage of the electrons and the radiation. This poses a lower bound for the pulse duration on the order of the cooperation length, defined as the slippage length in one exponential gain-length [14] (on the order of few fs to few hundred attoseconds at x-ray energies for typical experimental parameters). Similarly, the power of a high-gain FEL is limited to its saturation value, which is achieved as the electron beam approaches full microbunching [15]. Both effects are described in the one-dimensional (1D) theory of FELs by the Pierce parameter ρ , which defines the bandwidth, the efficiency, and gain-length of the system [15]. The cooperation length can be reduced and the saturation power increased by increasing the electron beam quality, but their ultimate values are always

tied to the universal scaling of the FEL dynamics with the Pierce parameter.

One regime of the FEL bypasses these limitations: the superradiant mode [16–20]. In this highly nonlinear regime, a short radiation pulse slips over the electrons at the speed of light, continuously extracting energy from fresh slices of the beam. In this regime, the interaction is so strong that the electrons become fully bunched as they interact with the rising edge of the pulse. This leads to amplification of the head of the pulse and absorption of the tail. The result is a soliton-like pulse that maintains a characteristic self-similar shape while growing in intensity and compressing in the time domain. Because the interaction is continuously sustained by new electrons, the superradiant mode has no saturation. Therefore, the peak power can grow indefinitely and the pulse duration can shrink well below the high-gain cooperation length. This regime was first experimentally observed at infrared wavelengths [21], and was extended to the XUV range [22] employing a harmonic cascade scheme [23, 24]. More recently, the superradiant regime has been observed in the context of cascaded x-ray FELs [25], resulting in terawatt-scale attosecond pulses. These experimental results call for a deeper understanding of the superradiant mode and its ultimate limits.

According to the existing 1D theory of superradiant FELs [26], the peak power grows quadratically with the propagation distance, z^2 , while the pulse duration shrinks as $z^{-1/2}$. However, we expect diffraction to dramatically change the superradiant behavior [27]. This is because the intensity on axis decreases as z^{-2} in a strongly diffracting beam, counteracting the quadratic gain predicted in 1D superradiance. In this letter, we report a new diffraction-dominated superradiant regime of the free-electron laser. In this regime, the pulse, closely coupled to the electron beam microbunching, develops into a soliton-like mode qualitatively similar to the 1D soliton. However, considering transverse diffraction

* riverr@stanford.edu

† marinelli@slac.stanford.edu

causes the on-axis intensity and pulse duration to change more slowly than in the 1D limit as diffraction losses nearly balance on-axis amplification, and the growth of the peak power is ultimately linear with z . We study this regime first using 3D FEL simulations. We then develop a self-consistent, asymptotic theory that accurately describes the duration, power and on-axis intensity of the superradiant pulse. Moreover, we find that the output pulse properties are weakly dependent on the initial conditions that launch the mode, suggesting superradiance as a route to short, intense, and stable pulses.

To introduce the qualitative features of the problem, Fig. 1 shows the results from a 3D simulation using the GENESIS 1.3 v4 code [28, 29] and the self-similar 1D solution starting from 0.5% initial bunching (see, for example, [30, 31]). The parameters used in the simulations are reported in Table I, with no emittance or energy spread in order to isolate the impact of diffraction from other complicating 3D effects. Furthermore, in all of the simulations that follow, the beam particles are loaded without shot noise (“quiet-loaded”) so as to highlight the superradiant physics in the asymptotic regime. Panel (a) shows the evolution of the power profile of the pulse in the 3D simulation with lineouts at three positions in the undulator. As the pulse propagates, the coherent gaussian seed gives rise to the expected superradiant profile characterized by a primary peak followed by a sequence of weak trailing peaks. Panel (b) shows the output power profile compared to that expected from the self-similar 1D solution. Panels (c) and (d) show the evolution of the on-axis intensity and full-width at half-maximum pulse duration in the two cases. The dashed curves showing the 1D results scale as z^2 and $z^{-1/2}$, respectively. In contrast, both the intensity and the duration begin to plateau in the 3D simulations. The transition from good agreement in the duration around 10 m to poor agreement thereafter indicates in particular that the pulse duration evolution is slower than the $1/\sqrt{z}$ dependence expected from the 1D theory. We note that in linear FEL theory, the effect of diffraction can be included in a pseudo 1D model by re-scaling the FEL equations to account for the longer wavelength [32, 33]. This approach does not work for the superradiant regime because of the lack of gain-guiding, as discussed in the Supplementary Information and illustrated in Fig. S1. Therefore a new theoretical approach is required to fully describe the physics at play.

We are interested in developing an asymptotic model of superradiant FELs in the diffraction dominated regime. We expect this regime to be realized when the interaction length z after the initial saturation is much larger than the typical length-scale of diffraction: $z \gg k_r \sigma_r^2$, where k_r is the radiation wavenumber and σ_r is the transverse beam size. The starting point for our theoretical model is the 3D FEL wave equation (see, for example, [12, 13, 30]):

$$\left(\frac{\partial}{\partial z} + \frac{1}{c} \frac{\partial}{\partial t} - \frac{1}{2ik_r} \nabla_{\perp}^2 \right) E_x(z, t, \mathbf{r}) = \kappa b(z, t) u(\mathbf{r}). \quad (1)$$

The coordinates z , t , and \mathbf{r} refer to the distance along the

Beam parameter	Value
Current I	4 (2) kA
Beam size σ_r	20 μm
Energy $\gamma_0 mc^2$	5 GeV
Undulator parameter	Value
Period $\lambda_u = 2\pi/k_u$	3.9 cm
Length L_u	80 (60) m
Resonant photon energy ($\hbar k_r c$)	540 eV
Seed field parameter	Value
FWHM power duration	0.5 fs
Peak intensity	1.27 (6.37) MW/ μm^2
Spot size w_0 [34]	70.7 μm

TABLE I. Parameters for simulations. Values given in parentheses are relevant for Fig. 2 and 3 where applicable. Other differences in later simulations are explicitly stated in the text.

undulator, time, and transverse coordinates, respectively. $E_x(z, t, \mathbf{r})$ is the slowly-varying envelope of the electric field, $b(z, t) = \langle e^{i\theta_j} \rangle$ is the bunching at a fixed location in the beam, where $\theta_j = (k_r + k_u)z - \omega_r t_j$ is the ponderomotive phase of the j -th electron, and $u(\mathbf{r})$ is the transverse profile of the beam normalized so that $\int d\mathbf{r} u(\mathbf{r}) = 1$. Finally, k_r is the radiation wavenumber, k_u is the undulator wavenumber, and the coupling term $\kappa = IK[\text{JJ}]/4\epsilon_0 c \gamma_0$, where K is the undulator strength parameter, I is the beam current, γ_0 is the beam Lorentz factor, and $[\text{JJ}]$ is the Bessel coupling factor [12, 13, 30]. Note that we are assuming that the bunching factor does not have an explicit transverse dependence. This approximation is appropriate in a diffraction-dominated case because the radiation mode is much larger than the electron beam and the field generating the bunching is roughly uniform over the transverse extent of the electron distribution.

The physical picture presented by the simulation and by intuitive arguments suggests that in the diffraction-dominated superradiant regime the pulse propagates at the speed of light with nearly constant on-axis intensity. This is similar to the 1D regime, where the pulse and beam microbunching both propagate at a velocity asymptotically approaching the speed of light, but with growing on-axis intensity [20]. We therefore assume that the electron dynamics depend strongly on the variable $\zeta = z - ct$, and have only a weak explicit dependence on z . Consequently we change variables from (z, t) to (z, ζ) and assume $b(z, t) \simeq b(\zeta)$. The resulting equation is formally equivalent to that of undulator radiation from a pre-bunched beam [35] and has the following solution:

$$E_x(z, \zeta, \mathbf{r}) = 2ib(\zeta)k_r\kappa \int \frac{d\mathbf{k}}{4\pi^2} e^{i\mathbf{k}\cdot\mathbf{r}} \frac{\tilde{u}(\mathbf{k})}{k^2} \left(1 - e^{\frac{ik^2 z}{2k_r}} \right) \quad (2)$$

where we have introduced the Fourier transform of the bunch shape $\tilde{u}(\mathbf{k}) = \int d\mathbf{r} e^{-i\mathbf{k}\cdot\mathbf{r}} u(\mathbf{r})$. The bunching $b(\zeta)$ can be determined self-consistently given this field and the equations of motion for the electrons. Written in terms of the relative energy deviation $\eta_j = (\gamma_j - \gamma_0)/\gamma_0$ and the ponderomotive phase $\theta_j = (k_r + k_u)z - \omega_r t_j$, the

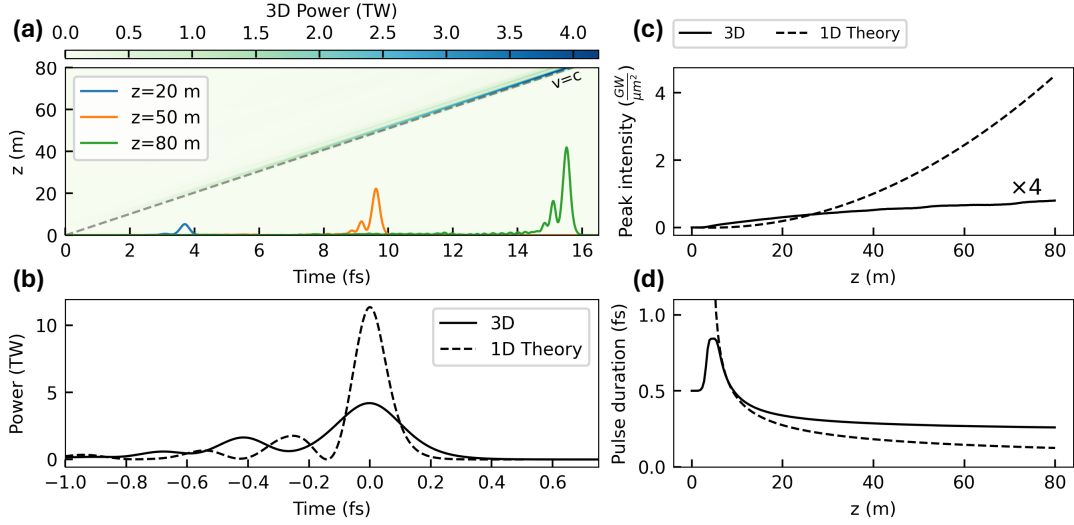


FIG. 1. Basic differences between superradiance with (3D) and without (1D) diffraction. (a) shows the evolution of pulse power over a 80 meter undulator with lineouts of the temporal profile at three positions. (b) shows the final power profile for the 1D and 3D cases. (c) and (d) show the peak intensity and pulse duration versus undulator length.

particles obey the pendulum equations:

$$\frac{d\theta_j}{dz} = 2k_u \eta_j \quad (3)$$

$$\frac{d\eta_j}{dz} = -\chi (E_x e^{-i\theta_j} + \text{c.c.}) \quad (4)$$

where $\chi = eK[\text{JJ}]/2\gamma_0^2 m c^2$ and the field must be evaluated at the position of particle j . In the diffraction-dominated regime, we assume that the field varies little over the beam area, and the particles move under the influence of the on-axis field. Using Eq. (2), for a gaussian beam with $u(\mathbf{r}) = \frac{1}{2\pi\sigma_r^2} e^{-\frac{r^2}{2\sigma_r^2}}$, the on-axis field is given by:

$$E_x(z, \zeta, \mathbf{0}) = ib(\zeta) k_r \kappa \frac{1}{2\pi} \ln \left(1 - \frac{iz}{k_r \sigma_r^2} \right) \quad (5)$$

Because the on-axis field only depends logarithmically on z , we will consider it constant during the interaction of a given electron with the short radiation pulse. In that case, a set of self-consistent equations can be written in terms of the collective variables $b = \langle e^{i\theta_j} \rangle$ and $P = \langle \eta_j e^{i\theta_j} \rangle$. Those collective variables equations include non-linear terms which are critical for capturing the superradiant physics properly. They can be evaluated using the methods described in [36] as shown in the supplementary, with the end result being a single second-order, nonlinear differential equation for the bunching:

$$\frac{d^2 b}{dx^2} - b + 3b|b|^2 = 0 \quad (6)$$

where $x = \sqrt{\frac{k_r \chi \kappa}{k_u} \frac{|\ln(1-iz/k_r \sigma_r^2)|}{2\pi}} 2k_r \zeta$. This equation is expected to be valid in the leading peak of the superradiant pulse. Equation (6) has an approximate solution

in terms of a hyperbolic secant [36]:

$$b(\zeta) \simeq \sqrt{\frac{2}{3}} \text{sech}(x - x_0) \quad (7)$$

This is reminiscent of both the hyperbolic secant solution found for the evolution of high-gain FELs in the early saturation regime [36], and in the case of 1D superradiance [31]. In what follows we will neglect the offset x_0 , since it only shifts the temporal profile. With this we can write a nearly self-consistent expression for the radiation field envelope,

$$E_x(z, \zeta, \mathbf{r}) \simeq 2i\kappa k_r \sqrt{\frac{2}{3}} \int \frac{d\mathbf{k}}{4\pi^2} e^{i\mathbf{k}\cdot\mathbf{r}} \frac{\tilde{u}(\mathbf{k})}{k^2} \left(1 - e^{\frac{ik_z z}{k_r}} \right) \times \text{sech} \left(\sqrt{\frac{k_r \chi \kappa}{k_u} \frac{|\ln(1-iz/k_r \sigma_r^2)|}{2\pi}} 2k_r \zeta \right) \quad (8)$$

This expression allows us to make predictions about key parameters: we will highlight the peak power, the maximal on-axis intensity, and the pulse duration. We will give formulas for a Gaussian transverse profile $u(r) = \frac{1}{2\pi\sigma_r^2} e^{-\frac{r^2}{2\sigma_r^2}}$ here, more details and derivations for different beam distributions are found in the supplementary material. First, the peak on-axis intensity and the full-width at half-maximum duration of the power and intensity asymptotically approach

$$I_{\max} = \frac{1}{3\epsilon_0 c} \left[\frac{IK[\text{JJ}]k_r}{4\pi\gamma_0} \left| \ln \left(1 - \frac{iz}{k_r \sigma_r^2} \right) \right| \right]^2 \quad (9)$$

$$\text{FWHM} = \frac{2\cosh^{-1}(\sqrt{2})}{\omega_r} \sqrt{\frac{\gamma}{|\ln(1-iz/k_r \sigma_r^2)|} \frac{I_A}{I} \frac{1 + \frac{K^2}{2}}{K^2[\text{JJ}]^2}} \quad (10)$$

where $I_A \simeq 17$ kA is the Alfvén current. The peak power asymptotically approaches

$$P_{\max} \simeq \frac{4\pi\sigma_r^2}{3\epsilon_0 c} \left(\frac{IK[\text{JJ}]k_r}{4\pi\gamma_0} \right)^2 \left[\frac{z}{k_r\sigma_r^2} \frac{\pi}{2} - 2 \ln \left(\frac{z}{k_r\sigma_r^2} \frac{e}{2} \right) \right] \quad (11)$$

These equations are similar in form to those found for the diffraction-dominated post-saturation regime of the high-gain FEL [35, 37, 38], reflecting the basic physics of emission from a pre-bunched beam that is at the core of both regimes.

These formulas and equation (8) can be considered a 0th order solution since we used the solution of the field which assumed the bunching to be constant. They are already quite accurate as we will see, but can be improved by iterating once more, plugging the bunching equation (7) back into the original wave equation with its explicit z dependence. This yields the field as

$$E_x(z, \zeta, \mathbf{r}) = \kappa \int \frac{d\mathbf{k}}{4\pi^2} e^{i\mathbf{k}\cdot\mathbf{r}} \tilde{u}(\mathbf{k}) \int_0^z dz' b(z', \zeta) e^{-\frac{ik^2}{2k_r}(z'-z)} \quad (12)$$

This change does not impact the peak power or intensity, but it will change the FWHM duration. In particular, the power and on-axis intensity profiles will now have slightly different temporal durations. This is because the radiation emitted on-axis is constantly slowly compressing, whereas the off-axis radiation which was emitted earlier is fixed at its original duration. The correct FWHM is found by evaluating the integrals in Eq. (12) as a function of ζ . Numerical fitting formulas for the FWHM corrections, valid for a wide range in $z/k_r\sigma_r^2$, are reported in the supplementary material.

We have derived these expressions in an asymptotic limit, using only the particular solution of the wave equation and neglecting entirely the initial conditions that launch the superradiant mode. That particular solution vanishes at $z = 0$, which we may refer to as the source point of the superradiant pulse. In reality, the seed pulse takes some time to launch the superradiant mode, creating an effective source point at $z = z_0 \neq 0$ (a similar issue is found in the 1-D theory). In the simulation results that follow we will show both our basic theory curves with $z_0 = 0$ and revised curves in which the effective z_0 is estimated by a linear fit to the power from the simulations. We will find that, in practice, the basic formulas with $z_0 = 0$ are more than sufficient to estimate the pulse properties, but accounting for z_0 makes the agreement nearly perfect.

We compare our results against 3D GENESIS simulations in Fig. 2. Panel (a) shows the output power profile after a sixty meter long undulator with an 11 micron beam size. The orange theory curve is the hyperbolic secant solution with the peak power and FWHM duration given by equations (11) and corrections from equation (12), and the orange dashed curve makes use of the z_0 estimate from the simulation. For reference, that

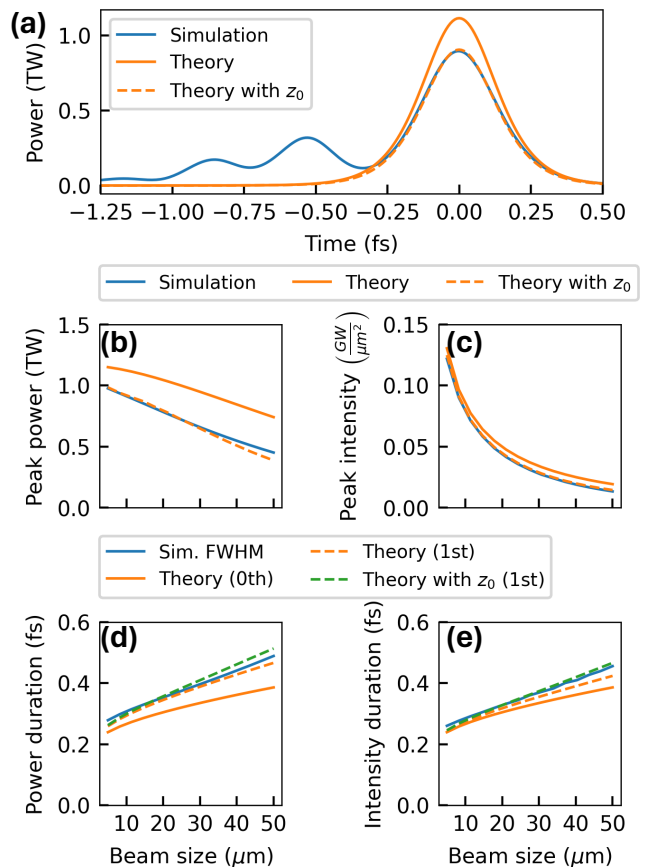


FIG. 2. Comparison of theory with GENESIS simulations with various beam sizes. (a) shows the temporal power and on-axis intensity profiles for an 11 micron beam size alongside the theoretical solutions. (b-d) show the output power, intensity, power duration, and intensity duration versus undulator length.

z_0 is 13 meters, meaning it takes 13 meters for the initial seed to launch the superradiant mode. Panels (b-e) show the peak power, peak intensity, and FWHM durations of power and on-axis intensity at the end of the sixty meter undulator as a function of beam size. In the FWHM curves we have now three theory curves: (0th) refers to the basic formulas not accounting for the slow z -dependence of the bunching equations (10), (1st) refers to revised formulas (12). We find excellent agreement in all parameters. Of particular note is that the intensity and duration predictions are quite good even without accounting for z_0 . This is because of their logarithmic dependence on z , whereas the peak power which varies asymptotically linearly with z experiences a larger shift from accounting for z_0 .

To further explore the role of the initial seed conditions on the behavior of the ultimate superradiant pulse, Fig. 3 shows simulation results for a fixed 20 μm beam size, and for a seed pulse with peak power ranging from 1 GW to 100 GW and FWHM duration between 0.2 and 0.6 fs. The same quantities are plotted as in Fig. 2, in the dura-

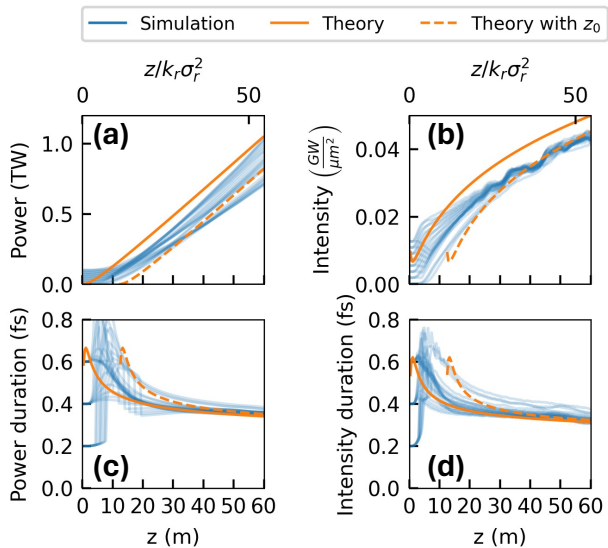


FIG. 3. Comparison of theory with GENESIS simulations showing peak power, intensity, and pulse duration along the undulator for a variety of seed powers and durations, as compared to the asymptotic theoretical behavior.

tion plots we now show only the 1st order theory curves. The z_0 used is the average for the 32 simulations. As expected from our previous discussion, the on-axis intensity and FWHM durations of both power and intensity all asymptotically approach the same logarithmically varying curves, nearly independent of the initial conditions. The power varies more due to its linear dependence on z_0 , a 12% rms fluctuation in these simulations, which is still quite small considering the two orders of magnitude variation in the seed power. This provides a path towards stabilizing the output of isolated attosecond XFELs, which suffer from significant shot-to-shot intensity fluctuations [6].

These 3D scaling laws are instructive for finding the best ways to utilize superradiance. Although superradiance has no saturation, the rest of the beam will be undergoing the usual FEL process driven by shot noise, referred to as self-amplified spontaneous emission (SASE).

Thus, in practice the superradiant solution is only practically utilizable before SASE saturates in the rest of the beam. One ideally wants to operate the FEL in a way that increases the SASE saturation length without strongly impacting the superradiant mode. For one example, our results indicate that the superradiant performance metrics are weak functions of the beam size, whereas the SASE gain length grows like $\sigma_r^{2/3}$. This implies that by increasing the beam size one can exponentially suppress SASE with minimal impact on superradiance. This is precisely what was found in the simulation and experimental results of [25]. Finally, our formulas provide a promising scaling for producing short pulses at high photon energies. For example, the diffraction-dominated superradiant pulse duration has a more favorable scaling with the beam energy and current compared to the shortest pulse duration achievable with the high-gain regime, proportional to $\lambda_r \sqrt{\gamma/I}$ for superradiance and $\lambda_r \gamma/I^{1/3}$ for the high-gain regime. These considerations can guide the field in the pursuit of ever shorter, higher power pulses.

We have presented the physics of a previously unstudied regime of the free-electron laser: diffraction-dominated superradiance. Through 3D simulations and a self-consistent theory of the nonlinear physics, we have shown that after sufficient propagation distance, superradiant free-electron lasers become limited by diffraction. In the limit that $z/k_r\sigma_r^2 > 1$, the pulse duration begins to shrink much more slowly than in the 1D case, like $1/\sqrt{|\ln(1 - iz/k_r\sigma_r^2)|}$, and the peak power begins to grow linearly rather than quadratically. These findings explain features of recent experiments with superradiant FELs and provide crucial information towards understanding the ultimate performance limits of superradiant FELs.

This work was supported by the U.S. Department of Energy, Office of Science, Office of Basic Energy Sciences under Contract No. DE-AC02-76SF00515, and by the U.S. Department of Energy, Office of Science, Office of Basic Energy Sciences Accelerator and Detector Research Program. The authors thank Zhirong Huang, Erik Hemming, Nicholas Sudar, and Filippo Sottocorona for helpful discussions.

-
- [1] P. Emma, R. Akre, J. Arthur, R. Bionta, C. Bostedt, J. Bozek, A. Brachmann, P. Bucksbaum, R. Coffee, F.-J. Decker, *et al.*, First lasing and operation of an ångstrom-wavelength free-electron laser, *nature photonics* **4**, 641 (2010).
- [2] T. Ishikawa, H. Aoyagi, T. Asaka, Y. Asano, N. Azumi, T. Bizen, H. Ego, K. Fukami, T. Fukui, Y. Furukawa, *et al.*, A compact x-ray free-electron laser emitting in the sub-ångström region, *nature photonics* **6**, 540 (2012).
- [3] H.-S. Kang, C.-K. Min, H. Heo, C. Kim, H. Yang, G. Kim, I. Nam, S. Y. Baek, H.-J. Choi, G. Mun, *et al.*, Hard x-ray free-electron laser with femtosecond-scale timing jitter, *Nature Photonics* **11**, 708 (2017).
- [4] W. Decking, S. Abeghyan, P. Abramian, A. Abramsky, A. Aguirre, C. Albrecht, P. Alou, M. Altarelli, P. Altmann, K. Amyan, *et al.*, A mhz-repetition-rate hard x-ray free-electron laser driven by a superconducting linear accelerator, *Nature photonics* **14**, 391 (2020).
- [5] E. Prat, R. Abela, M. Aiba, A. Alarcon, J. Alex, Y. Arbelo, C. Arrell, V. Arsov, C. Bacellar, C. Beard, *et al.*, A compact and cost-effective hard x-ray free-electron laser driven by a high-brightness and low-energy electron beam, *Nature Photonics* **14**, 748 (2020).
- [6] J. Duris, S. Li, T. Driver, E. G. Champenois, J. P.

- MacArthur, A. A. Lutman, Z. Zhang, P. Rosenberger, J. W. Aldrich, R. Coffee, *et al.*, Tunable isolated attosecond x-ray pulses with gigawatt peak power from a free-electron laser, *Nature Photonics* **14**, 30 (2020).
- [7] Z. Zhang, J. Duris, J. P. MacArthur, A. Zholents, Z. Huang, and A. Marinelli, Experimental demonstration of enhanced self-amplified spontaneous emission by photocathode temporal shaping and self-compression in a magnetic wiggler, *New Journal of Physics* **22**, 083030 (2020).
- [8] S. Huang, Y. Ding, Y. Feng, E. Hemsing, Z. Huang, J. Krzywinski, A. Lutman, A. Marinelli, T. Maxwell, and D. Zhu, Generating single-spike hard x-ray pulses with nonlinear bunch compression in free-electron lasers, *Physical review letters* **119**, 154801 (2017).
- [9] A. Marinelli, J. MacArthur, P. Emma, M. Guetg, C. Field, D. Kharakh, A. Lutman, Y. Ding, and Z. Huang, Experimental demonstration of a single-spike hard-x-ray free-electron laser starting from noise, *Applied Physics Letters* **111** (2017).
- [10] J. T. O’Neal, E. G. Champenois, S. Oberli, R. Obaid, A. Al-Haddad, J. Barnard, N. Berrah, R. Coffee, J. Duris, G. Galinis, *et al.*, Electronic population transfer via impulsive stimulated x-ray raman scattering with attosecond soft-x-ray pulses, *Physical review letters* **125**, 073203 (2020).
- [11] S. Kuschel, P. J. Ho, A. A. Haddad, F. Zimmermann, L. Flueckiger, M. R. Ware, J. Duris, J. P. MacArthur, A. Lutman, M.-F. Lin, *et al.*, Enhanced ultrafast x-ray diffraction by transient resonances, *arXiv preprint arXiv:2207.05472* (2022).
- [12] C. Pellegrini, A. Marinelli, and S. Reiche, The physics of x-ray free-electron lasers, *Reviews of Modern Physics* **88**, 015006 (2016).
- [13] Z. Huang and K.-J. Kim, Review of x-ray free-electron laser theory, *Physical Review Special Topics-Accelerators and Beams* **10**, 034801 (2007).
- [14] R. Bonifacio, L. De Salvo, P. Pierini, N. Piovella, and C. Pellegrini, Spectrum, temporal structure, and fluctuations in a high-gain free-electron laser starting from noise, *Physical review letters* **73**, 70 (1994).
- [15] R. Bonifacio, C. Pellegrini, and L. Narducci, Collective instabilities and high-gain regime in a free electron laser, *Optics Communications* **50**, 373 (1984).
- [16] R. Bonifacio and F. Casagrande, The superradiant regime of a free electron laser, *Nuclear Instruments and Methods in Physics Research Section A: Accelerators, Spectrometers, Detectors and Associated Equipment* **239**, 36 (1985).
- [17] R. Bonifacio, B. McNeil, and P. Pierini, Superradiance in the high-gain free-electron laser, *Physical Review A* **40**, 4467 (1989).
- [18] R. Bonifacio, N. Piovella, and B. McNeil, Superradiant evolution of radiation pulses in a free-electron laser, *Physical Review A* **44**, R3441 (1991).
- [19] L. Giannessi, P. Musumeci, and S. Spampinati, Nonlinear pulse evolution in seeded free-electron laser amplifiers and in free-electron laser cascades, *Journal of Applied Physics* **98** (2005).
- [20] X. Yang, N. Mirian, and L. Giannessi, Postsaturation dynamics and superluminal propagation of a superradiant spike in a free-electron laser amplifier, *Physical Review Accelerators and Beams* **23**, 010703 (2020).
- [21] T. Watanabe, X. Wang, J. Murphy, J. Rose, Y. Shen, T. Tsang, L. Giannessi, P. Musumeci, and S. Reiche, Experimental characterization of superradiance in a single-pass high-gain laser-seeded free-electron laser amplifier, *Physical review letters* **98**, 034802 (2007).
- [22] N. S. Mirian, M. Di Fraia, S. Spampinati, F. Sottocorona, E. Allaria, L. Badano, M. B. Danailov, A. Demidovich, G. De Ninno, S. Di Mitri, *et al.*, Generation and measurement of intense few-femtosecond superradiant extreme-ultraviolet free-electron laser pulses, *Nature Photonics* **15**, 523 (2021).
- [23] L. Giannessi, M. Artioli, M. Bellaveglia, F. Briquez, E. Chiadroni, A. Cianchi, M. Couprie, G. Dattoli, E. Di Palma, G. Di Pirro, *et al.*, High-order-harmonic generation and superradiance in a seeded free-electron laser, *Physical review letters* **108**, 164801 (2012).
- [24] L. Giannessi, M. Bellaveglia, E. Chiadroni, A. Cianchi, M. Couprie, M. Del Franco, G. Di Pirro, M. Ferrario, G. Gatti, M. Labat, *et al.*, Superradiant cascade in a seeded free-electron laser, *Physical review letters* **110**, 044801 (2013).
- [25] P. Franz *et al.*, Terawatt-scale attosecond x-ray pulses from a cascaded superradiant free-electron laser, *Accepted by Nature Photonics* (2024).
- [26] R. Bonifacio, L. D. S. Souza, P. Pierini, and N. Piovella, The superradiant regime of a fel: analytical and numerical results, *Nuclear Instruments and Methods in Physics Research Section A: Accelerators, Spectrometers, Detectors and Associated Equipment* **296**, 358 (1990).
- [27] L. Giannessi, C. R. Frascati, P. Musumeci, and S. Spampinati, Non Linear Pulse Evolution in Seeded and Cascaded FELs, in *Proc. FEL’05* (JACoW Publishing, Geneva, Switzerland).
- [28] S. Reiche, Genesis 1.3: a fully 3d time-dependent fel simulation code, *Nuclear Instruments and Methods in Physics Research Section A: Accelerators, Spectrometers, Detectors and Associated Equipment* **429**, 243 (1999).
- [29] S. Reiche, Genesis-1.3-version4, <https://github.com/svenreiche/Genesis-1.3-Version4> (2022).
- [30] K.-J. Kim, Z. Huang, and R. Lindberg, *Synchrotron radiation and free-electron lasers* (Cambridge university press, 2017).
- [31] N. Piovella, A hyperbolic secant solution for the superradiance in free electron lasers, *Optics communications* **83**, 92 (1991).
- [32] L. Giannessi, Overview of Perseo, a System for Simulating FEL Dynamics in Mathcad, in *Proc. FEL’06* (JACoW Publishing, Geneva, Switzerland) pp. 91–94.
- [33] M. Xie, Design optimization for an x-ray free electron laser driven by slac linac, in *Proceedings Particle Accelerator Conference*, Vol. 1 (IEEE, 1995) pp. 183–185.
- [34] A. E. Siegman, *Lasers* (University science books, 1986).
- [35] E. L. Saldin, E. A. Schneidmiller, and M. V. Yurkov, A simple method for the determination of the structure of ultrashort relativistic electron bunches, *Nuclear Instruments and Methods in Physics Research Section A: Accelerators, Spectrometers, Detectors and Associated Equipment* **539**, 499 (2005).
- [36] E. Hemsing, Simple model for the nonlinear radiation field of a free electron laser, *Physical Review Accelerators and Beams* **23**, 120703 (2020).
- [37] W. Fawley, “optical guiding” limits on extraction efficiencies of single-pass, tapered wiggler amplifiers, *Nuclear Instruments and Methods in Physics Research Section A: Accelerators, Spectrometers, Detectors and Associated*

- Equipment **375**, 550 (1996).
- [38] E. A. Schneidmiller and M. Yurkov, Optimization of a high efficiency free electron laser amplifier, Physical Review Special Topics-Accelerators and Beams **18**, 030705 (2015).

Supplementary Information: Three-dimensional theory of superradiant free-electron lasers

River R. Robles,^{1,2,3,*} Luca Giannessi,^{4,5} and Agostino Marinelli^{1,3,†}

¹*SLAC National Accelerator Laboratory, Menlo Park, CA 94025*

²*Stanford University, Department of Applied Physics, Stanford, CA 94305*

³*Stanford PULSE Institute, SLAC National Accelerator Laboratory, Menlo Park, CA 94025, USA*

⁴*Elettra-Sincrotrone Trieste, 34149 Basovizza, Trieste, Italy*

⁵*ENEA C.R. Frascati, 00044 Frascati (Roma), Italy*

(Dated: March 19, 2024)

arXiv:2403.02153v2 [physics.acc-ph] 18 Mar 2024

* riverr@stanford.edu

† marinelli@slac.stanford.edu

I. 1D SELF-SIMILAR SOLUTION WITH DIFFRACTION CORRECTION

The 1D self-similar solutions are produced using an initial bunching of 0.5%. Figure S1 shows similar results as Figure 1 in the main text, only now we have added an extra theory line corresponding to the diffraction-corrected 1D theory. We note that the theory curves are shifted in z to overlap roughly the first $1/\sqrt{z}$ -like decay around 10 meters. This has the effect of reducing the peak power and intensity while increasing the pulse duration, however it does not change the fundamentally different scalings between the 1D and 3D cases. The diffraction-corrected 1D power still grows quadratically and the pulse duration still shrinks as $1/\sqrt{z}$, both in clear contrast to the 3D simulations.

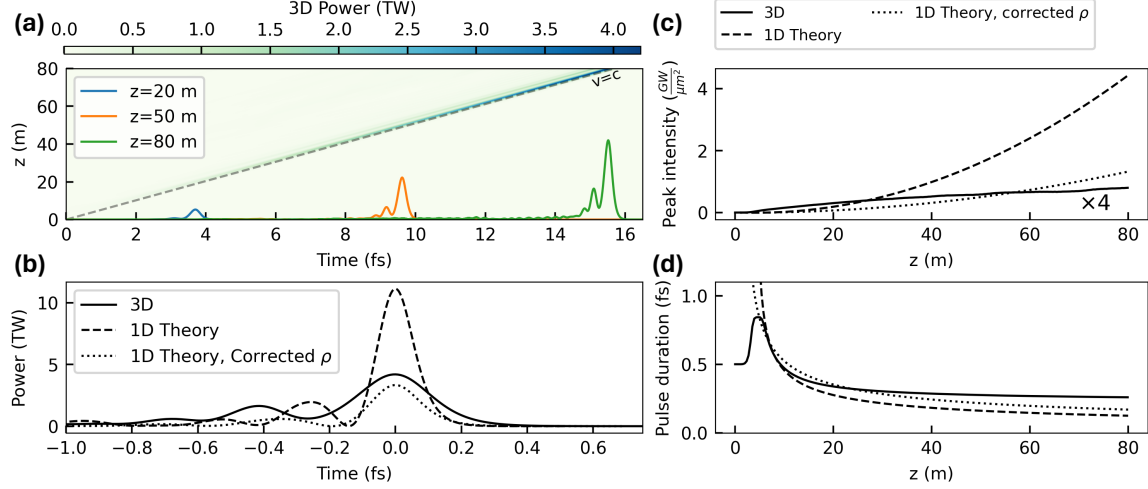


FIG. S1: Same as Fig. 1 in the main text. 3D simulations of an 80 meter undulator are compared to the 1D self-similar solution, now including a version scaled according to the diffraction-corrected value of the Pierce parameter.

II. EXTENDED DERIVATIONS

A. Calculation of the field for unknown bunching

In this section we will provide a more detailed derivation of the expressions in the main text. We start from the FEL wave equation given in the main text as

$$\left(\frac{\partial}{\partial z} + \frac{1}{c} \frac{\partial}{\partial t} - \frac{1}{2ik_r} \nabla_{\perp}^2 \right) E_x(z, t, \mathbf{r}) = \kappa b(z, t) u(\mathbf{r}) \quad (\text{S1})$$

If we move from t to $\zeta = z - ct$, then $\partial_z + \partial_{ct} = \partial_z$. Furthermore, we'll move to angular space transversely by introducing the Fourier transform $\tilde{E}_x(z, t, \mathbf{k}) = \int d\mathbf{r} e^{-i\mathbf{k}\cdot\mathbf{r}} E_x(z, t, \mathbf{r})$. The wave equation becomes

$$\left(\frac{\partial}{\partial z} + \frac{k^2}{2ik_r} \right) \tilde{E}_x(z, \zeta, \mathbf{k}) = \kappa b(\zeta) \tilde{u}(\mathbf{k}) \quad (\text{S2})$$

where $k^2 = \mathbf{k} \cdot \mathbf{k}$. Since we are assuming that $b(z, t)$ is a function only of ζ in this first analysis, this equation can be solved directly. That solution is

$$\tilde{E}_x(z, \zeta, \mathbf{k}) = 2ik_r \kappa b(\zeta) \frac{\tilde{u}(\mathbf{k})}{k^2} \left(1 - e^{\frac{ik^2 z}{2k_r}} \right) \quad (\text{S3})$$

By inverting the Fourier transform we find the spatial representation of the field,

$$E_x(z, \zeta, \mathbf{r}) = 2ik_r \kappa b(\zeta) \int \frac{d\mathbf{k}}{4\pi^2} e^{i\mathbf{k}\cdot\mathbf{r}} \frac{\tilde{u}(\mathbf{k})}{k^2} \left(1 - e^{\frac{ik^2 z}{2k_r}} \right) \quad (\text{S4})$$

For ease of later calculations it is convenient to specialize this expression to the case of an axisymmetric beam, $u(\mathbf{r}) = u(r)$. For that we can write

$$E_x(z, \zeta, \mathbf{r}) = 2ik_r \kappa b(\zeta) \int \frac{dk}{2\pi} J_0(kr) \frac{\tilde{u}(k)}{k} \left(1 - e^{\frac{ik^2 z}{2k_r}}\right) \quad (\text{S5})$$

As we explained in the text, the particle dynamics are affected by the on-axis field in the asymptotic diffraction-dominated limit. For a gaussian beam $u(r) = \frac{1}{2\pi\sigma_r^2} e^{-\frac{r^2}{2\sigma_r^2}}$ and $\tilde{u}(k) = e^{-\frac{k^2\sigma_r^2}{2}}$, and the on-axis field is

$$E_x(z, \zeta, \mathbf{0}) = ik_r \kappa b(\zeta) \frac{1}{2\pi} \ln \left(1 - \frac{iz}{k_r \sigma_r^2}\right) \equiv ik_r \kappa b(\zeta) \frac{1}{2\pi} \left| \ln \left(1 - \frac{iz}{k_r \sigma_r^2}\right) \right| e^{-i\phi(z)} \quad (\text{S6})$$

where the phase is defined as $\phi(z) = -\arg \left[\ln \left(1 - iz/k_r \sigma_r^2\right) \right]$. Similarly, we can write the on-axis field for a hard-edge cylindrical beam with $u(r) = \frac{1}{\pi R^2}$ for $r < R$. In this case $\tilde{u}(k) = 2J_1(kR)/kR$, and

$$E_x(z, \zeta, \mathbf{0}) = 2ik_r \kappa b(\zeta) \frac{1}{4\pi} \left[\Gamma_0 \left(\frac{ik_r R^2}{2z} \right) - \frac{2iz}{k_r R^2} \left(1 - e^{-\frac{ik_r R^2}{2z}}\right) \right] \simeq ik_r \kappa b(\zeta) \frac{1}{2\pi} \left| \ln \left(1 - \frac{3iz}{k_r R^2}\right) \right| e^{-i\phi(z)} \quad (\text{S7})$$

where now $\phi(z) = -\arg \left[\ln \left(1 - 3iz/k_r R^2\right) \right]$ – in other words, the on-axis field in the hard-edge case is very similar to that of the gaussian case with the substitution $\sigma_r \rightarrow R/\sqrt{3}$

B. Scaling and solution of the particle motion

Given this field, we can proceed to studying the particle dynamics to self-consistently determine the bunching. The pendulum equations for the particles are

$$\frac{d\eta_j}{dz} = -\chi (E_x e^{-i\theta_j} + \text{c.c.}) \quad (\text{S8})$$

$$\frac{d\theta_j}{dz} = 2k_u \eta_j \quad (\text{S9})$$

We are interested in solving the dynamics of a single slice at some fixed ponderomotive phase variable θ_0 . The reason we only need to track the dynamics of one slice is precisely because the bunching depends only on ζ – it means that when properly scaled, the dynamics of all slices are equivalent. In terms of the ponderomotive phase, we may write $\zeta = z - ct = \frac{\theta_0 - k_u z}{k_r}$, implying that for fixed θ_0 we can relate the derivatives $\frac{d}{dz} = -\frac{k_u}{k_r} \frac{d}{d\zeta}$. Thus we can write

$$\frac{d\eta_j}{d\zeta} = \frac{k_r}{k_u} k_r \kappa \chi \frac{|\ln(1 - iz/k_r \sigma_r^2)|}{2\pi} \left(ib(\zeta) e^{-i(\theta_j + \phi(z))} + \text{c.c.} \right) \quad (\text{S10})$$

$$\frac{d\theta_j}{d\zeta} = -2k_r \eta_j \quad (\text{S11})$$

The form of these equations suggests scaling to the variables $x = 2k_r \zeta \sqrt{\frac{k_r}{k_u} \kappa \chi \frac{|\ln(1 - iz/k_r \sigma_r^2)|}{4\pi}}$ and $p_j = \eta_j / \sqrt{\frac{k_r}{k_u} \kappa \chi \frac{|\ln(1 - iz/k_r \sigma_r^2)|}{4\pi}}$, where we assume that during the passage of the short superradiant pulse over this slice of the beam the logarithm may be treated as constant. Note that this means that the on-axis field phase $\phi(z)$ is also roughly constant over the timescale of the electron dynamics. These scalings are reminiscent of those used in 1D superradiant theory, only in the 1D case it would have gone like $\sqrt{z\zeta}$ instead of $\sqrt{\ln(z)\zeta}$. In this scaling we have

$$\frac{dp_j}{dx} = ib(x) e^{-i(\theta_j + \phi(z))} + \text{c.c.} \quad (\text{S12})$$

$$\frac{d\theta_j}{dx} = -p_j \quad (\text{S13})$$

These equations can now be used to self-consistently describe the bunching in the beam. Before we do that analytically, we should discuss the phase $\phi(z)$. Just like the amplitude the phase varies logarithmically with z , so it can similarly be treated as constant during the dynamics of one slice. Even more than that, as $z \rightarrow \infty$, this phase approaches zero. We can see the phase and its impact on the particle dynamics in Fig. S2. In panel (a) we plot the phase $\phi(z) = -\arg(\ln(1 - iz/k_r \sigma_r^2))$ for $10 < \frac{z}{k_r \sigma_r^2} < 10^4$. We see that it is slowly but monotonically decreasing, and over this range of three orders of magnitude it varies from 0.55 down to 0.15. To place that magnitude in context we show

in panel (b) the results of tracking simulations employing the scaled pendulum equations (S12)-(S13). In particular we initiate 4,096 particles and solve these equations numerically for phase ϕ varying from 0 to $\pi/2$ and for a fixed initial bunching of 0.1%. In panel (b) we are plotting the peak bunching and the width of the rising edge of that bunching in x . We observe that in general the dynamics vary weakly with ϕ , and especially for $\phi < 0.5$ radians there is nearly no difference, most notably a 3% increase in the width of the bunching which is negligible for our current considerations. With these justifications we will proceed simply ignoring the phase term $\phi(z)$.

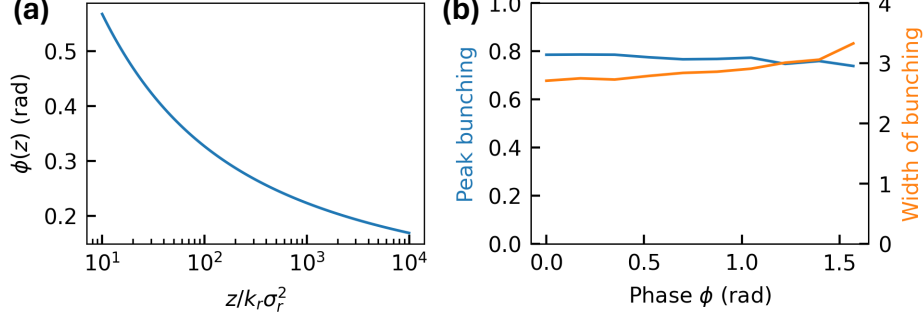


FIG. S2: Impact of the field phase $\phi(z)$ on the particle dynamics. (a) $\phi(z)$ for $z/k_r \sigma_r^2$ varying from 10 to 10^4 . (b) Peak bunching and bunching width from macroparticle tracking simulations for varying phase $\phi(z)$.

To study the dynamics of the particles up to the first peak of the superradiant pulse we can employ the nonlinear collective variables method developed in [?]. To do so we need to introduce the collective energy modulation $P = \langle p_j e^{i\theta_j} \rangle$. We can then write equations of motion for the bunching and for P ,

$$\frac{db}{dx} = i \left\langle \frac{d\theta_j}{dx} e^{i\theta_j} \right\rangle = -iP \quad (\text{S14})$$

$$\frac{dP}{dx} = \left\langle \frac{dp_j}{dx} e^{i\theta_j} + ip_j \frac{d\theta_j}{dx} e^{i\theta_j} \right\rangle = ib - ib^* \langle e^{2i\theta_j} \rangle - i \langle p_j^2 e^{i\theta_j} \rangle \quad (\text{S15})$$

It has been shown that up through the early saturation regime of the FEL, the following scalings approximately hold: $\langle e^{2i\theta_j} \rangle \simeq \langle e^{i\theta_j} \rangle^2 = b^2$ and $\langle p_j^2 e^{i\theta_j} \rangle \simeq \langle p_j^2 \rangle \langle e^{i\theta_j} \rangle = \langle p_j^2 \rangle b$. The energy spread $\langle p_j^2 \rangle$ can be determined by evaluating its equation of motion,

$$\frac{d\langle p_j^2 \rangle}{dx} = 2 \langle ib p_j e^{-i\theta_j} - ib^* p_j e^{i\theta_j} \rangle = 2i (bP^* - b^*P) = 2 \frac{d|b|^2}{dx} \quad (\text{S16})$$

from which it follows the conservation law $\frac{d}{dx} (\langle p_j^2 \rangle - 2|b|^2) = 0$. Assuming vanishing initial energy spread and bunching, this means that that $\langle p_j^2 \rangle = 2|b|^2$. Plugging this into the expression for $\frac{dP}{dx}$ and combining it with the expression for $\frac{db}{dx}$, we find a single second-order nonlinear differential equation for the bunching

$$\frac{d^2 b}{dx^2} - b + 3b|b|^2 = 0 \quad (\text{S17})$$

This equation is very nearly the same nonlinear Duffing equation studied by Hemsing in [?]. We will approach it in the same way he did. We start by noting that in the linear regime (the leading edge of the superradiant pulse), this equation reads $\frac{d^2 b}{dx^2} = b$, with exponential solutions of the form $e^{\pm x}$. Of particular note is that the solution is purely real, or more accurately it has constant phase. In Hemsing's case, his linear regime solution was the typical linear FEL solutions which have linearly varying phase, so he assumed his field to have a linear phase as well. We will assume that the phase of b is constant through the first synchrotron oscillation (first superradiant peak), writing $b = B e^{i\phi_0}$. In that case we have

$$\frac{d^2 B}{dx^2} - B + 3B^3 = 0 \quad (\text{S18})$$

and this is now precisely the nonlinear Duffing equation studied by Hemsing. The solution is given in terms of the cosine-like Jacobi elliptic function as

$$B(x) = Y \text{cn}(\kappa^2 x + \psi | n) \quad (\text{S19})$$

The parameters Y , κ and n are defined by

$$Y^2 = \frac{\alpha \pm \sqrt{(\alpha - \beta B_0^2)^2 + 2\beta(B'_0)^2}}{\beta} \quad (\text{S20})$$

and

$$\kappa^2 = \beta Y^2 - \alpha \quad n = \frac{\beta Y^2}{2\kappa^2} \quad (\text{S21})$$

where $\alpha = 1$ and $\beta = 3$ for our case. B_0 and B'_0 are the initial conditions, which we will find to have a minimal impact on our results. In particular, we will assume $B_0, B'_0 \ll 1$ so that we may write approximately

$$Y^2 \simeq \frac{2}{3} + (B'_0)^2 - B_0^2 \quad (\text{S22})$$

$$\kappa^2 \simeq 1 + 3((B'_0)^2 - B_0^2) \quad (\text{S23})$$

$$n \simeq 1 - \frac{3}{2}((B'_0)^2 - B_0^2) \quad (\text{S24})$$

For small initial conditions, then we have $Y \simeq \sqrt{2/3}$, $\kappa \simeq 1$, and $n \simeq 1$. For $n \simeq 1$, the cosine-like Jacobi elliptic function behaves like a hyperbolic secant, $\mathbf{cn}(x|n \simeq 1) \simeq \text{sech}(x)$. These allow us to write the approximate result

$$B(x) \simeq \sqrt{\frac{2}{3}} \text{sech}(x) \quad (\text{S25})$$

where we have neglected the offset ψ since we are not concerned with the specific location of the peak, only its value and width.

C. Properties of the field in the first solution iteration

It follows that we can write the field up to a constant phase factor as

$$E_x(z, \zeta, \mathbf{r}) = 2ik_r \kappa \sqrt{\frac{2}{3}} \text{sech} \left(2k_r \zeta \sqrt{\frac{k_r}{k_u} \kappa \chi \frac{|\ln(1 - iz/k_r \sigma_r^2)|}{4\pi}} \right) \int \frac{dk}{2\pi} J_0(kr) \frac{\tilde{u}(k)}{k} \left(1 - e^{\frac{ik^2 z}{2k_r}} \right) \quad (\text{S26})$$

Let us now compute several properties of this field. First, both the on-axis intensity and the power will depend on ζ as the square of the sech function. The full-width at half-maximum of $\text{sech}^2(x)$ is $2\cosh^{-1}(\sqrt{2})$, so it follows that the FWHM temporal width is

$$\text{FWHM} = \frac{2\cosh^{-1}(\sqrt{2})}{\omega_r} \sqrt{\frac{\gamma}{|\ln(1 - iz/k_r \sigma_r^2)|} \frac{I_A}{I} \frac{1 + \frac{K^2}{2}}{K^2 [\text{JJ}]^2}} \quad (\text{S27})$$

Note that this is the same for the hard-edge cylindrical beam as long as $\sigma_r \rightarrow R/\sqrt{3}$, as before.

The maximal on-axis intensity on the pulse is given by

$$I_{\max} = 2\epsilon_0 c |E_x(z, 0, \mathbf{0})|^2 = \frac{1}{3\epsilon_0 c} \left[\frac{IK[\text{JJ}]k_r}{4\pi\gamma_0} \left| \ln \left(1 - \frac{iz}{k_r \sigma_r^2} \right) \right| \right]^2 \quad (\text{S28})$$

and the peak power is

$$P_{\max} = \int 2\epsilon_0 c |E_x(z, 0, \mathbf{r})|^2 d\mathbf{r} = \frac{4}{3\epsilon_0 c} \left(\frac{IK[\text{JJ}]k_r}{\gamma_0} \right)^2 \int \frac{d\mathbf{k}}{2\pi} \frac{\tilde{u}(k)^2}{k^3} \sin^2 \left(\frac{k^2 z}{4k_r} \right) \quad (\text{S29})$$

For the gaussian beam this is

$$P_{\max} = \int 2\epsilon_0 c |E_x(z, 0, \mathbf{r})|^2 d\mathbf{r} = \frac{4\pi\sigma_r^2}{3\epsilon_0 c} \left(\frac{IK[\text{JJ}]k_r}{4\pi\gamma_0} \right)^2 \left[\frac{z}{k_r \sigma_r^2} \arctan \left(\frac{z}{2k_r \sigma_r^2} \right) - 2\coth^{-1} \left(1 + \frac{8k_r^2 \sigma_r^4}{z^2} \right) \right] \quad (\text{S30})$$

$$\simeq \frac{4\pi\sigma_r^2}{3\epsilon_0 c} \left(\frac{IK[\text{JJ}]k_r}{4\pi\gamma_0} \right)^2 \left[\frac{z}{k_r \sigma_r^2} \frac{\pi}{2} - 2 \ln \left(\frac{z}{k_r \sigma_r^2} \frac{e}{2} \right) \right] \quad (\text{S31})$$

For a hard-edge beam the integral can be evaluated but the result is a long sequence of hypergeometric functions. We will just give the asymptotic approximation:

$$P_{\max} = \frac{2\pi R^2}{3\epsilon_0 c} \left(\frac{IK[\text{JJ}]k_r}{4\pi\gamma_0} \right)^2 \left[\pi \frac{z}{k_r R^2} - \ln \left(2e^{\gamma - \frac{5}{3}} \frac{z}{k_r R^2} \right) \right] \quad (\text{S32})$$

where γ is again Euler's constant.

III. CORRECTIONS TO THE FWHM FORMULAS

Numerical corrections to the simpler formula for the duration of the superradiant pulse can be written with the following fitting functions, which are accurate within 1% over four orders of magnitude of the dimensionless diffraction parameter $z/k_r\sigma_r^2$ ($3 < \frac{z}{k_r\sigma_r^2} < 10^4$):

$$\frac{\text{FWHM}_{\text{power}}}{\text{FWHM}_0} \simeq 0.995 + \frac{0.628}{0.27 + |\ln(1 - iz/k_r\sigma_r^2)|} \quad (\text{S33})$$

$$\frac{\text{FWHM}_{\text{intensity}}}{\text{FWHM}_0} \simeq 0.973 + \frac{0.254}{-0.64 + |\ln(1 - iz/k_r\sigma_r^2)|} \quad (\text{S34})$$